Title	Horizontally oriented molecular thin films for application in organic solar cells
Author(s)	Matsushima, Toshinori; Matsuo, Hitoshi; Yamamoto, Tetsuo; Nakao, Akichika; Murata, Hideyuki
Citation	Solar Energy Materials and Solar Cells, 123: 81-91
Issue Date	2014-01-29
Type	Journal Article
Text version	author
URL	http://hdl.handle.net/10119/13011
Rights	Copyright (C) 2014, Elsevier. Licensed under the Creative Commons Attribution-NonCommercial-NoDerivatives 4.0 International license (CC BY-NC-ND 4.0). [http://creativecommons.org/licenses/by-nc-nd/4.0/] NOTICE: This is the author's version of a work accepted for publication by Elsevier. Toshinori Matsushima, Hitoshi Matsuo, Tetsuo Yamamoto, Akichika Nakao, Hideyuki Murata, Solar Energy Materials and Solar Cells, 123, 2014, 81-91, http://dx.doi.org/10.1016/j.solmat.2014.01.004
Description	

JAIST

JAPAN
ADVANCED INSTITUTE OF
SCIENCE AND TECHNOLOGY

Japan Advanced Institute of Science and Technology

Horizontally oriented molecular thin films for application in organic solar cells

Toshinori Matsushima, Hitoshi Matsuo, Tetsuo Yamamoto,

Akichika Nakao, Hideyuki Murata*

School of Materials Science, Japan Advanced Institute of Science and Technology,

1-1 Asahidai, Nomi, Ishikawa 923-1292, Japan

* Corresponding author. Tel.: +81 761 51 1531; fax: +81 761 51 1149

E-mail address: murata-h@jaist.ac.jp (H. Murata)

ABSTRACT

The authors investigate the influence of molecular orientation of *p*-type molecules of alpha-sexithiophene (α-6T) and *n*-type molecules of 3,4,9,10-perylene tetracarboxylic bisbenzimidazole (PTCBI) on organic solar cell (OSC) performance. Deposition of α-6T and subsequently PTCBI on an α-6T buffer surface rubbed with a nylon cloth allows their horizontal orientations to be formed in separate layers. Power conversion efficiency and operation stability of a rubbed OSC are markedly improved when compared with an unrubbed OSC. The improved OSC performance is confirmed to be

due to increases in light absorption, exciton diffusion length, energy difference between the *p*-type and *n*-type layers, and carrier collection by electrodes, which are caused by the rubbing-induced double horizontal orientations.

Graphical abstract
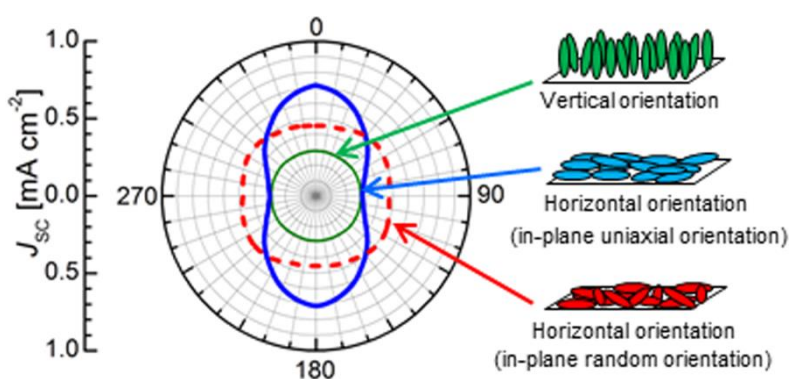
Highlights

► Influence of molecular orientation on organic solar cell performance is investigated.

► A rubbing technique induces double horizontal orientations of α-6T and PTCBI.

► The horizontal orientations enhance efficiency and operation stability of the cell.

► The improved cell performance is discussed in terms of molecular orientation.

1. Introduction

Performance of organic (opto)electronic devices, such as organic light-emitting diodes (OLED), organic solar cells (OSC), and organic thin-film transistors (OTFT), has rapidly progressed through synthesis of new organic materials, exploration of new device architectures, and elucidation of device working mechanisms. In addition, considerable effort has recently been devoted to control molecular orientation to achieve higher device performance. It is known that for OTFTs a vertical orientation of molecules with their molecular axes stacked parallel to each other on a substrate surface enhances carrier mobility in the stacking direction due to enhanced π coupling between neighboring molecules [1,2]. For standard OLEDs and OSCs where a current flow takes place normal to the substrate plane, a horizontal orientation of molecules with respect to the substrate plane is more desirable for a current flow than the vertical orientation [3,4]. The horizontal orientation increases light out-coupling efficiency of OLEDs [5] and light-harvesting efficiency of OSCs [6] due to alignment of molecular electronic transition moments parallel to the substrate plane. Moreover it is known that ionization potential energy (IP) and electron affinity (EA) of organic films are dependent by several hundred meV upon molecular orientation [7-10], indicating that a charge injection barrier at metal/organic and organic/organic heterojunction interfaces as well

as an energy difference between a highest occupied molecular orbital (HOMO) level of a *p*-type material and a lowest unoccupied molecular orbital (LUMO) level of an *n*-type material, which is correlated to open-circuit voltage of OSCs [11], are controllable by molecular orientation. We have recently demonstrated that a rubbing-induced horizontal orientation of alpha-sexithiophene (α-6T) markedly reduces a driving voltage of OLEDs due to a reduced hole injection barrier [10,12]. Thus, the appropriately controlled molecular orientation is very advantageous to improve device performance.

Deposition of an organic film on a specific surface (e.g., a KCl single-crystal surface [3], a copper iodide (CuI)-coated substrate surface [13], an oriented molecular surface [4], and a periodic groove surface [14]) has been used to control molecular orientation. Besides, quasi-homoepitaxial growth of organic molecules on a surface, where the same or different kind of molecule is pre-oriented by a rubbing technique, is also possible to obtain a horizontal orientation of organic molecules [6,15-17]. Unique OLED and OSC characteristics have been realized by using the oriented molecular films. For examples, Videlot *et al.* fabricated Schottky cells based on octithiophene (8T) and showed a substantial increase in photocurrent by aligning 8T molecules horizontally and parallel to each other on a substrate by means of a rubbing technique [6]. Era *et al.* used

quasi-homoepitaxial growth of *p*-sexiphenyl (6P) on a rubbed 6P surface to obtain an

uniaxially and horizontally oriented 6P film, resulting in polarized electroluminescence

observed from the oriented 6P film although performance of a rubbed OLED was the

same as that of an unrubbed OLED [16]. Yanagi *et al.* constructed OLEDs by depositing

6P and additional layers on a KCl (001) surface and transferring the multilayer structure

to an indium tin oxide (ITO)-coated substrate [3]. A horizontal orientation of 6P,

deposited at a lower temperature, resulted in a lower drive voltage than a vertical

orientation. Tanaka *et al.* obtained uniaxially and horizontally oriented PTCBI by

depositing PTCBI on a rubbed PTCBI surface. They used the oriented PTCBI film to

fabricate an image sensor that works under polarized light irradiation by utilizing a

difference in photocurrent [17]. Chen *et al.* found that copper phthalocianine (CuPc)

molecules were horizontally oriented on a CuI surface although CuPc molecules were

vertically oriented on a bare glass substrate [13]. OSC performance was higher when

using the horizontally oriented CuPc than the vertically oriented CuPc. Moreover

Yokoyama *et al.* demonstrated that planar-shaped long organic molecules in

vacuum-deposited amorphous films were horizontally oriented by themselves without

any influence of substrate surfaces [18], enabling higher-performance OSCs to be

realized [19]. However in the above-mentioned reports, horizontally oriented molecules

were formed in a single organic layer, so that the enhancing effect of the single horizontal orientation on the device performance is limiting. If both *p*-type and *n*-type molecules can be horizontally oriented in each layer of a multilayer structure simultaneously, OSC performance will be further enhanced because the enhancing effect caused by two kinds of horizontal orientation in the separate *p*-type and *n*-type layers becomes doubled when compared with the case of the single horizontal orientation.

In this study we show results of OSCs where both *p*-type molecules of α-6T and *n*-type molecules of 3,4,9,10-perylene tetracarboxylic bisbenzimidazole (PTCBI) are horizontally oriented in separate layers by growing α-6T quasi-homoepitaxially and subsequently PTCBI quasi-heteroepitaxially on an α-6T buffer layer that is mechanically rubbed with a nylon cloth. We obtain about three times improvement of power conversion efficiency (η) by using the rubbing technique. To investigate reasons for the improved η, we analyze the α-6T and PTCBI films with ultraviolet/visible (UV-VIS) absorption spectroscopy, atomic force microscopy (AFM), a photoluminescence (PL)-quenching technique [20,21], and photoelectron yield spectroscopy (PYS) and fabricate hole-only α-6T devices and electron-only PTCBI

devices. As the results of the analyses, we find that the improved η arises from increases in absorbance, exciton diffusion length, HOMO-LUMO energy difference, and hole and electron collection by respective electrodes, which are caused by the double horizontal orientations of α-6T and PTCBI on the rubbed surface. We believe that the results obtained in this study are very useful for opening a way to design higher-performance OSCs and for clarifying working mechanisms of OSCs as well as basic optical, electronic and electrical characteristics of oriented molecular films.

2. Experimental

2.1. Materials

Figure 1 shows the molecular structures of α-6T and PTCBI, which were used as model materials for fabrication of OSCs to investigate how their molecular orientations affect OSC performance. A strong intermolecular interaction between these sorts of flat molecule lead to efficient quasi-epitaxial growth [6,17]. α-6T (Aldrich) and PTCBI (Luminescence Technology) were purchased and purified twice with a temperature-gradient vacuum train sublimation technique prior to deposition. Other materials of 2,9-dimethyl-4,7-diphenyl-1,10-phenanthroline (BCP) (Nippon Steel Chemical), CuPc (Nippon Steel Chemical), MoO_3 (Mitsuwa Chemical), Ag (Nilaco),

and Al (Nilaco) were used as purchased because they were already refined grades.

2.2. Substrate cleaning

Fused silica substrates and glass substrates coated with a 150 nm ITO layer having a sheet resistance of 10 ohms per square (Sanyo Vacuum Industries) were cleaned by ultrasonication in acetone, followed by ultrasonication in detergent, pure water, and isopropanol (for 10 min each). The substrates were further cleaned with UV-ozone treatment (PL21-200, SEN LIGHT) for 30 min. After the treatment, the cleaned substrates were immediately transferred into a vacuum chamber (E-200, ALS technology) to thermally deposit organic films on the cleaned substrates under a base pressure of 10^{-5} Pa.

2.3. Vacuum deposition of organic films on rubbed surfaces

The sample preparation scheme is illustrated in (1)-(8) of Fig. 1. The three-step technique was used to control molecular orientation [6,16,17]. In the first step, a 15 nm α-6T film was vacuum-deposited on the cleaned fused silica substrate at a deposition rate of 0.1 nm s^{-1} (see (1) in Fig. 1). After the deposition, the α-6T film was directly transferred from the vacuum chamber to an adjacent nitrogen-filled glove box

(KK-011-EXTRA, KIYON) (O_2 and H_2O levels were below 1 ppm). In the second step, the α-6T film was 16 times rubbed in a given direction (uniaxial rubbing) with a 3.5 cm-diameter cylindrical vial wound with a dust-less nylon cloth ((2) and (4) in Fig. 1). This rubbing number was the optimized value that allowed the most horizontally oriented α-6T film to be obtained (this result will be published elsewhere). Besides the above-mentioned standard uniaxial rubbing, the multiaxial rubbing was tested ((3) and (4) in Fig. 1), i.e., the pre-deposited α-6T film was rubbed 16 times in various directions in the numerical order shown in (3) of Fig. 1. The angle between the neighboring multiaxial rubbing directions was 11.25˚. The films were uniaxially and multiaxially rubbed by hand, so that the rubbing condition was not controlled precisely but the transfer speed and the weight of the vial on the film were roughly 25 cm s^{-1} and 500 g, respectively. The rubbed α-6T films were returned to the vacuum chamber. In the third step, a 50 nm α-6T film was quasi-homoepitaxially grown on the bare fused silica surface and the uniaxially and multiaxially rubbed α-6T surfaces at a deposition rate of 0.01 nm s^{-1} ((5) and (6) in Fig. 1). Then a 30 nm PTCBI film was quasi-heteroepitaxially grown on top of the above-mentioned 50 nm α-6T films at a deposition rate of 0.01 nm s^{-1} ((7) and (8) in Fig. 1). The deposition rates and the film thickness were controlled with a carefully calibrated quartz crystal microbalance. The

substrate temperature during the organic deposition was not controlled (room temperature) and measured at nearly 14 °C before the organic deposition but this temperature does not increase significantly under our deposition condition [22]. The films thus prepared were characterized with UV-VIS absorption spectroscopy (V670, JASCO) in air.

2.4. Fabrication of solar cells

The stack of a 50 nm α-6T *p*-type layer and a 30 nm PTCBI *n*-type layer was prepared on the bare ITO surface and the ITO surfaces covered with the uniaxially and multiaxially rubbed α-6T buffer layers with the same preparation condition. Then, a 10 nm BCP exciton-blocking layer [23] and a 100 nm Ag electrode layer were vacuum-deposited on top of the PTCBI layers to complete the OSCs, whose structures are shown in (9) and (10) of Fig. 1. The deposition rates were set at 0.1 nm s^{-1} for BCP and 0.3 nm s^{-1} for Ag. The active device area was 2.125 mm^{-2}. The fabricated OSCs were encapsulated with a glass cap and an UV curing epoxy resin together with a dessicant sheet to avoid OSC degradation in air. Current density-voltage (*J-V*) characteristics of the unrubbed and rubbed OSCs were measured with a computer-controlled sourcemeter (2400, Keithley) under AM1.5 solar illumination at

100 mW cm^{-2} (one sun) from a solar simulator (LHX-500E3, Koken Kogyo). Monochrome light from a Xe lamp equipped with a monochromer (SM-25S-1, Bunkoukeiki) was irradiated to the OSCs to calculate incident photon-to-collected electron efficiency (IPCE) at various wavelengths from a generated photocurrent and a monochrome light power measured with a power meter (FieldMaxII-TO and OP-2 UV, Coherent Inc.).

2.5. Sample preparation for measuring exction diffusion length

The exciton diffusion length L of α-6T and PTCBI was measured with the PL-quenching technique [20,21]. Films of α-6T and PTCBI with different thickness d were prepared on the bare fused silica and rubbed surfaces (see the sample structures (11)-(14) in Fig. 1). The rubbed PTCBI used to prepare these samples was obtained by depositing a 15 nm PTCBI film on the fused silica substrate at a deposition rate of 0.1 nm s^{-1} and uniaxially or multiaxialy rubbing this PTCBI film 16 times with the nylon cloth in the manners similar to (2) and (3) of Fig. 1. Films of PTCBI and CuPc with the thickness of 5 nm were deposited on top of the above-mentioned α-6T and PTCBI films, respectively. They were used as exciton-quenching layers because efficient charge-transfer dissociation occurs at the quenching interfaces of α-6T/PTCBI and

11

PTCBI/CuPc as a result of good positional relations of their HOMO and LUMO levels

(see Refs [20,21] and energy-level diagrams shown in Fig. 7). Since radii (R_0) of

Förster-type energy transfer from α-6T to PTCBI and from PTCBI to CuPc are

relatively small (R_0 calculation is discussed in Sec. 2.3), the charge-transfer dissociation

of excitons that diffuse and reach the quenching interfaces is much more dominant than

the exciton quenching by long-distance energy transfer. Excitation light of 365 nm

wavelength from an UV LED (ZUV-C30H and ZUV-H20MB, OMRON) was irradiated

to the samples from the substrate side to measure PL spectra of α-6T and PTCBI in the

presence and absence of the quenching layers with a photo-detector (C7473,

Hamamatsu). Details of the PL-quenching technique will be explained later.

2.6. Sample preparation for measuring ionization potential energy and AFM images

The films of α-6T (50 nm) and PTCBI (30 nm) were deposited on the bare ITO

surface and the ITO surfaces covered with the rubbed α-6T buffer films (see (15)-(16)

in Fig. 1). These samples were used to estimate IP of α-6T and PTCBI simultaneously

with PYS (AC-2 Riken Keiki). During the PYS measurement, ITO was grounded to

reduce electrical charging of the organic surfaces. Surface morphology of the 50 nm

α-6T films in the absence of PTCBI was evaluated with AFM (VN-8000, KEYENCE).

2.7. Fabrication of hole-only and electron-only devices

The hole-only α-6T devices and the electron-only PTCBI devices were constructed with the same preparation condition described before (the device structures are shown in (17)-(20) of Fig. 1). The deposition rates were 0.05 nm s^{-1} for MoO$_3$ and 0.3 nm s^{-1} for Al. The active device area was 2.125 mm^{-2}. To investigate the electrical characteristics of the oriented α-6T and PTCBI films, dark *J-V* characteristics of the devices were measured with the Keithley 2400 sourcemeter after the device encapsulation.

3. Results and discussion

3.1. Molecular orientation

We already reported the molecular orientation characteristics of the unrubbed and rubbed α-6T films alone [12,24]. Namely, although as-deposited α-6T molecules are vertically oriented on the substrate [25,26], we found that the uniaxial rubbing resulted in a change from vertical to horizontal orientations of α-6T and alignment of its long molecular axes along the rubbing direction while average α-6T thickness markedly reduced from 15 to 2-3 nm after the rubbing. Deposition of additional α-6T on the

uniaxially rubbed α-6T surface is expected to allow horizontally and uniaxially oriented

α-6T molecules to be formed in the overlying film due to a quasi-homoepitaxial growth

effect [6,15-17]. However the horizontally and uniaxially oriented α-6T film does not

effectively absorb light of an electric field vector perpendicular to the α-6T alignment

direction, giving rise to a problem of reduced photon absorption in the direction. To

overcome this problem, we tried to use the multiaxial rubbing to obtain the film where

α-6T is horizontally oriented and orientation directions of each α-6T crystallite are

random in the film plane. It is expected that in-plane randomly oriented α-6T molecules

are obtained in the overlying α-6T film deposited on the multiaxially rubbed surface. To

verify such molecular orientation characteristics, the UV-vis absorption spectra of α-6T

deposited on the unrubbed and rubbed surfaces were measured under unpolarized and

polarized light incidence normal to the substrate plane.

The UV-vis absorption spectra (unpolarization) of the 50 nm α-6T films deposited

on the bare fused silica surface and the uniaxially and multiaxially rubbed α-6T surfaces

(samples (5) and (6) in Fig. 1) are shown in Fig. 2(a). The absorption in this wavelength

range originates from π-π^* transition of α-6T having an electronic transition moment

along its long molecular axis [25]. The relatively strong absorption peak at ≈360 nm and

the weak vibronic side in the 400-600 nm wavelength range can be assigned to aggregated and unaggregated α-6T molecules, respectively [24,26]. One famous example for appearance of such a short-wavelength peak is formation of H-aggregates. The absorbance was increased about twice in the whole wavelength range by depositing α-6T on the uniaxially and multiaxially rubbed surfaces, indicating that vertically oriented α-6T is converted into horizontally oriented α-6T to some extent by the rubbing technique, i.e., the number of horizontally oriented α-6T molecules deposited on the rubbed surfaces is doubled. Since absorbance of the uniaxially and multiaxially rubbed α-6T films alone was lower by ≈1/30 than that of the overlying 50 nm α-6T films deposited on the rubbed surfaces, the spectra shown in Fig 2(a) reflect the light absorption by the overlying films more dominantly than by the underlying rubbed films.

Figure 2(b) shows the substrate angle dependence of absorbance of the α-6T films at 360 nm, which was measured by rotating the substrate under normal incidence of polarized light. The 0-180˚ direction shown in this figure corresponds to the uniaxial rubbing direction and the first rubbing direction of the multiaxial rubbing. The absorbance of the α-6T film deposited on the bare fused silica surface (sample (5)) showed a completely isotropic angular distribution, indicating that α-6T molecules are

15

completely in-plane random while the vertical orientation is dominant. The absorbance

parallel to the rubbing direction was much larger than that perpendicular in the α-6T

film deposited on the uniaxially rubbed surface (sample (6)), indicating that most of

horizontally oriented α-6T molecules are aligned along the rubbing direction. On the

other hand, since the less angular dependence of the absorbance was observed from the

α-6T film deposited on the multiaxially rubbed surface (sample (6)), α-6T molecules of

this film look almost like in-plane random. The areas of the angle dependence of the

uniaxially and multiaxially rubbed samples were larger than that of the angle

dependence of the unrubbed sample. This observation again suggests that the

quasi-homoepitaxial growth of α-6T on the uniaxially and multiaxially rubbed α-6T

surfaces enables the number of horizontally oriented molecules to be increased.

The PTCBI film (30 nm) was vacuum-deposited on the horizontally oriented

α-6T films to investigate whether the quasi-heteroepitaxial growth of PTCBI molecules

is possible or not. The UV-vis absorption spectra and the substrate angle dependence of

absorbance of the PTCBI samples (7) and (8) (Fig. 1) at 670 nm are shown in Fig. 2(c)

and 2(d), respectively. PTCBI has an electronic transition moment along its long

molecular axis [17]. In the short-wavelength region below 600 nm, α-6T absorption and

PTCBI absorption are largely overlapped. There is PTCBI absorption only in the long-wavelength region over 600 nm. In this region, the absorbance of PTCBI was increased ≈1.5 times by depositing PTCBI on the horizontally oriented α-6T films, indicating that the horizontal orientation of PTCBI is enhanced due to the quasi-heteroepitaxial growth effect. The total increase in the absorbance of both α-6T and PTCBI at 400 nm of the short-wavelength region was a factor of ≈2, which is similar to the value obtained from the α-6T films alone because PTCBI absorption is very weak at 400 nm. The angle dependence of the absorbance at 670 nm, where PTCBI absorption only is present, showed the characteristics similar to those observed in Fig. 2(b). In other words, PTCBI molecules are in-plane randomly oriented in the unrubbed sample and the multiaxially rubbed sample, but PTCBI molecules are mostly aligned along the rubbing direction in the uniaxially rubbed sample. The observed horizontal orientations of the films of α-6T and PTCBI lead to efficient light absorption, resulting in an increase in short-circuit current density (J_{SC}) of OSCs.

It has been reported that the horizontally oriented molecules gradually reduce in a large thickness region distant from the substrate surface [6]. Also it is probable that our unitiaxially and multiaxially rubbed samples do not have homogeneous crystallites

containing horizontally oriented molecules only, but have heterogeneous crystallites where the horizontal and vertical orientations still coexist [24]. We would like to mention that the molecular orientation characteristics discussed in the present study are the averaged characteristics of the films containing such orientational gradient and heterogeneous crystallites.

2.2. OSC characteristics

The *J-V* characteristics of the unrubbed and rubbed OSCs (the OSC structures (9) and (10) shown in Fig. 1) under the AM1.5 solar irradiation of 100 mW cm^{-2} are shown Fig. 3(a). The V_{OC}, J_{SC}, fill factor (FF), η, series resistance (R_S), and shunt resistance (R_{SH}) of the OSCs are summarized in Table 1. The R_S and R_{SH} are respectively estimated from the *J-V* slopes near the V_{OC} and J_{SC} points. Unrubbed OSCs of various α-6T and PTCBI thickness were fabricated (glass substrate/ITO (150 nm)/α-6T (20-70 nm)/PTCBI (10-50 nm)/BCP (10 nm)/Ag (100 nm)). As the results, the highest η was obtained when using 50 nm α-6T and 30 nm PTCBI. We thereby chose the optimized thickness for the OSC fabrication.

We obtained about three times improvement of η from $\approx$0.4% to $\approx$1.2% in the

18

uniaxially and multiaxially rubbed OSCs when compared with the unrubbed OSC. The

V_{OC}, J_{SC}, and FF were increased from ≈0.38 to ≈0.68 V by ≈79%, from ≈1.70 to ≈2.77

mA cm^{-2} by ≈63%, and from ≈0.61 to ≈0.65 by ≈7%, respectively, by using the uniaxial

and multiaxial rubbing. One of the reasons for the increase in J_{SC} is the increase in

absorbance of α-6T and PTCBI as discussed before. The other reasons will be discussed

later. Leakage current seems not to increase in the rubbed OSCs because the R_{SH} is

almost unchanged among all OSCs.

The J_{SC} of the OSCs was measured by rotating the substrate under polarized solar

light incidence normal to the substrate plane (Fig. 3(b)). After passing the solar light

through a polarizer, the total optical power density of the solar light was reduced to ≈1/3

of the initial value (≈33 mW cm^{-2}) and a shape of the solar light spectrum was slightly

shaved below 400 nm due to absorption of the polarizer itself. The substrate angle

dependence of J_{SC} was consistent with the molecular orientation characteristics after the

rubbing (see Fig. 2(b) and 2(d)), meaning that J_{SC} measured under the polarized solar

light is strongly dependent upon the molecular orientation. The dichroic ratio of J_{SC}

measured from the uniaxially rubbed OSC is 2.4, which is an intermediate value

between the absorbance dichroic ratios of the uniaxially rubbed α-6T and PTCBI

samples (4.3 and 2.2, respectively) but is closer to the latter value because photons absorbed in PTCBI mainly contribute to photocurrent (see Fig. 3(d)).

It is difficult to allow light of an electric field vector perpendicular to a molecular alignment axis to be absorbed effectively by an in-plane uniaxially aligned molecular film. Therefore, we attempted to do the multiaxial rubbing to obtain an in-plane randomly oriented molecular film that can effectively absorb light in every direction. This attempt is successful as can be seen from the results shown in Fig. 2. However, the performances of the uniaxially and multiaxially rubbed OSCs were almost similar (Table 1), which contradicts our initial expectation. Since our α-6T and PTCBI films have low absorbance, most of incident photons pass through the films without absorption. In this case, the increase in light absorption of the 0-180˚ direction cancels out the decrease in light absorption of the 90-270˚ direction in the in-plane uniaxially aligned molecular films (see Fig. 2(b) and 2(d)). Therefore the reason for the similar OSC performances is probably that a total light absorption extent by the in-plane uniaxially aligned molecular films is similar to that by the in-plane randomly oriented molecular films. We suggest that the in-plane random orientation caused by the multiaxial rubbing we proposed here will be more useful to enhance future OSC

performance than the in-plane uniaxial orientation if in-plane randomly oriented molecular films, whose thickness is large or absorption coefficient is high enough to absorb most of incident photons, can be used in OSCs.

The plots of IPCE and J_{SC} at various wavelengths are shown in Fig. 3(c) and 3(d), respectively. The J_{SC} in Fig. 3(d) was calculated from the IPCE and an unpolarized AM1.5 solar spectrum. The IPCE and J_{SC} were increased in the whole wavelength region by the rubbing, in part due to the increase in absorbance of α-6T and PTCBI. The IPCE in the short-wavelength region was much higher than that in the long-wavelength region because exciton diffusion length of α-6T is much longer than that of PTCBI (see Sec 2.3). Despite the higher IPCE in the short-wavelength region, the J_{SC} in the long-wavelength region became higher, indicating that photon absorption in PTCBI contributes to J_{SC} more predominantly than α-6T because solar light intensity is stronger at long wavelengths. Moreover we confirmed that the total J_{SC} estimated from the integral of Fig. 3(d) almost agreed with J_{SC} estimated from the J-V curves of Fig. 3(a).

Our OSCs discussed in this study were fabricated using the dust-less nylon cloth

in the clean nitrogen-filled glove box without exposing them to air. However when the multiaxially rubbing was done in air, the η significantly reduced by $\approx$41% (see Table 1), probably due to contamination of the films by dusts, oxygen, or water. Thus the rubbing of the films in the clean condition is a key to improve OSC performance by the rubbing technique.

The unpolarized AM 1.5 solar light of 100 mW cm^{-2} was continuously irradiated to the OSCs at an initial optimum operation point to evaluate their time stability of V_{OC}, J_{SC}, FF and η (Fig. 4(a), 4(b), 4(c) and 4(d), respectively). The continuous solar light irradiation resulted in a gradual reduction in FF and η while V_{OC} and J_{SC} were not changed significantly. It is noteworthy that the degradation speeds of the uniaxially and multiaxially rubbed OSCs are lower than that of the unrubbed OSC, demonstrating the effectiveness of the rubbing technique for the practical OSC application. The deposition of α-6T and PTCBI on the rubbed surfaces significantly change not only absorbance but also various characteristics of the bulk films (see Sec 2.3, 2.5, and 2.6). Although we still do not know a detailed reason for the improved OSC stability, the changes in the bulk characteristics is probably related to the OSC stability. We need further investigation to clarify why the OSC stability is improved by the rubbing technique.

2.3. Exciton diffusion length

The exciton diffusion length L of organic films can be measured with the PL-quenching technique [20]. When assuming that an organic film of thickness d has one quenching interface, at which charge-transfer dissociation of excitons occurs, and the other is completely non-quenching, the L is expressed by the equation,

$$\frac{PL_1}{PL_2} = 1 - \frac{L[1 - \exp(-2d/L)]}{d[1 + \exp(-2d/L)]}, \quad (1)$$

where PL_1 and PL_2 are PL intensity in the presence and absence of a quenching interface, respectively. The PL_1/PL_2 ratio is measured as a function of d. Then, by fitting a PL_1/PL_2 vs d plot with the equation, one can estimate L.

The PL-quenching characteristics of the unrubbed and rubbed α-6T samples (11) and (12) (Fig. 1) were evaluated to estimate their L. The α-6T films show three PL peaks at $\approx$550, $\approx$590, and $\approx$640 nm, where a PL peak from PTCBI is not present. The PL intensity of α-6T was reduced by depositing the PTCBI exciton quencher on the α-6T films. The PL intensity in the presence of PTCBI (PL_1) was divided by that in the absence of PTCBI (PL_2) to calculate the PL_1/PL_2 ratios at various α-6T thickness d (Fig. 5(a)). The smaller PL_1/PL_2 ratios observed from the rubbed samples than the unrubbed

sample indicates that excitons generated in horizontally oriented α-6T is more strongly quenched by PTCBI than in vertically oriented α-6T due to longer L normal to the substrate. Fitting the experimental PL_1/PL_2-d plots (symbols) with the equation (1) (solid curves) yields $L=13.9\pm0.7$ nm for the unrubbed sample, $L=18.8\pm2.0$ nm for the multiaxially rubbed film, and $L=20.1\pm1.7$ nm for the multiaxially rubbed sample.

The L of PTCBI was also measured with the same PL-quenching technique ((13) and (14) in Fig. 1). In this case, CuPc deposited on PTCBI was used as an exciton quencher. The PL peak of PTCBI was located at ≈840 nm. The substrate-normal L is estimated to be $L=2.8\pm0.3$ nm for the unrubbed sample, $L=5.5\pm0.5$ nm for the uniaxially rubbed film, and $L=5.3\pm0.9$ nm for the multiaxially rubbed film by the fitting Fig. 5(b) with the equation. The L estimated from the unrubbed PTCBI sample is consistent with the previous reports (≈3 nm) [20,21]. Note that our PTCBI is a mixture of cis and trans isomers, which are known to have different crystalline structures, exciton diffusion length, and OSC characteristics [21].

From the aforementioned PL-quenching results, it is clear that the L of α-6T is much higher than that of PTCBI, resulting in the higher IPCE in the short-wavelength

region. Moreover, the substrate-normal L is found to increase ≈ 1.4 times for α-6T and ≈ 1.9 times for PTCBI by the uniaxial and multiaxial rubbing due to the enhanced π coupling between horizontally oriented molecules. This result indicates that excitons of horizontaly oriented α-6T and PTCBI effectively reach the donor/acceptor interface, leading to the increase in J_{SC} as well.

The equation (1) is valid when excitons that diffuse and reach the donor/acceptor interfaces are quenched. However, exciton quenching by long-distance energy transfer from donor to acceptor molecules is also possible to explain the variation of the PL_1/PL_2 ratios. The R_0 of Förster-type energy transfer from a donor molecule to an acceptor molecule is given by the equation [27],

$$R_0^6 = \frac{9000(\ln 10)\kappa^2 \phi}{128\pi^6 n^4 N_A} \int_0^\infty f_D(\lambda)\varepsilon_A(\lambda)\lambda^4 d\lambda , \quad (2)$$

where κ^2 is the dipole orientation factor that varies between 0 and 4, ϕ is the PL quantum yield of a donor, n is the refractive index of a medium, N_A is Avogadro's number, $f_D(\lambda)$ is the normalized donor emission spectrum, $\varepsilon_A(\lambda)$ is the acceptor molar extinction coefficient, and λ is the light wavelength. When both donor and acceptor molecules are horizontally oriented relative to a substrate surface as observed in this study, the R_0 becomes high because the κ^2 and ε_A increase. Therefore, there is a

possibility that the smaller PL_1/PL_2 ratios observed from the rubbed samples (Fig. 5(a) and 5(b)) are not caused by the increase in L but the increase in R_0. To verify this point we calculated the R_0 to be 1.5 nm for the α-6T donor→PTCBI acceptor Förster energy transfer and 0.9 nm for the PTCBI donor→CuPc acceptor Förster energy transfer when using κ^2=4 (a parallel dipole orientation of donor and acceptor molecules), ϕ=0.025% (α-6T donor) and 0.003% (PTCBI donor) [28], n=1.7 (a standard value for organic films) [29,30], and ε_A=32690 M^{-1} cm^{-1} at λ_{max}=550 nm (PTCBI acceptor) and 25780 M^{-1} cm^{-1} at λ_{max}=620 nm (CuPc acceptor) [31]. Since the ε_A used here was estimated from absorption spectra of the PTCBI and CuPc acceptor films deposited on fused silica substrates, actual ε_A of the PTCBI and CuPc acceptors deposited on the horizontally oriented α-6T and PTCBI donor surfaces must be higher than the above-mentioned values because horizontal orientations of the PTCBI and CuPc acceptor molecules are induced by the underlying α-6T and PTCBI donor layers. When assuming that the ε_A of the PTCBI and CuPc acceptors increases twice due to their horizontal orientations, the R_0 slightly increases from 1.5 to 1.6 nm (α-6T donor→PTCBI acceptor Förster energy transfer) and from 0.9 to 1.0 nm (PTCBI donor→CuPc acceptor Förster energy transfer). The ε_A no longer affect the R_0 significantly because Eq. (2) includes the sixth-root expression. In either case, the estimated R_0 values are overestimated due to the highest

κ^2 we used here, but are relatively small in comparison with the d variation in Fig. 5(a) and 5(b), indicating that the Förster-type energy transfer between the donor and acceptor molecules is not so big problem for the present L calculation using the PL quenching technique

2.4. Surface morphology

Results of AFM exhibited that grooves were formed and surface roughness was increased when rubbing the α-6T films although the as-deposited α-6T film had no groove structure [6,12,24]. After the deposition of the additional 50 nm α-6T film on these rubbed surfaces, the groove structure became less clearly visible and the surface roughness became relatively flat (see the AFM images and cross sectional profiles images in Fig. 6). The surface roughness parameter (R_a) is calculated to be 6.1 nm for the unrubbed α-6T sample, 7.3 nm for the uniaxially rubbed α-6T sample, and 7.4 nm for the multiaxially rubbed α-6T sample, respectively, from the AFM images. Bulkheterojunction and nanostructured OSCs have been adopted to induce efficient charge separation as a result of a larger donor/acceptor interface area [32,33]. We assume that the α-6T/PTCBI interface area does not affect the improved OSC performance because the surface roughness is not changed significantly between the

unrubbed and rubbed samples.

2.5. HOMO and LUMO levels

The photoelectron yield spectra of the stacked samples (15) and (16) (Fig. 1) are shown in Fig. 7(a). The long mean free path of photoexcited electrons with very low kinetic energy in PYS enables detection of photoelectron emission from different two kinds of molecule at the same time [34], i.e., there are two photoelectron emission onsets in the spectra. The first and second onsets correspond to photoelectron emission from α-6T and PTCBI, respectively. The IP was found to increase by ≈0.28 eV for α-6T and by ≈0.14 eV for PTCBI. It has been reported that a direction and magnitude of a surface dipole built into an organic layer depend on molecular orientation and they strongly affect a molecular electronic structure such as IP and EA [7-10]. Duhm et al. has shown that a change from vertical to horizontal orientations of α-6T increases its IP by ≈0.4 eV due to the modified surface dipole [9], which agrees with our results. Therefore, we assume that the increase in IP originates from the horizontal orientations of α-6T and PTCBI formed in the films. The bigger increase in IP was observed from the α-6T films than the PTCBI films, probably because more efficient vertical-to-horizontal orientation conversion occurs in the α-6T films than in the PTCBI

films as discussed before.

The HOMO and LUMO levels of α-6T and PTCBI, which were estimated from the IP and absorption onset energy, are depicted in Fig. 7(b). The absorption onset energies seem to be independent of the molecular orientations (see Fig. 2(a) and 2(c)), indicating that the widths of band gaps of α-6T and PTCBI are unchanged. Therefore, the HOMO and LUMO levels downshift spontaneously as shown in Fig. 7(b) due to the increases in IP. The actual LUMO levels may be located above the estimated LUMO levels because exciton binding energy is not taken into account for the LUMO estimation. The difference in the HOMO level of α-6T and the LUMO level of PTCBI is roughly estimated to be 0.64 eV for the unrubbed sample and 0.78-0.79 eV for the uniaxially and multiaxially rubbed samples, meaning that the HOMO-LUMO difference increases by ≈0.15 eV. It is well known that V_{OC} is strongly correlated to such HOMO/LUMO difference although V_{OC} is empirically lower by ≈0.3 eV than the HOMO/LUMO difference [11,35]. Therefore we believe that the increase in V_{OC} observed from our rubbed OSCs is in part due to the increased HOMO-LUMO difference.

2.6. Hole and electron transport

The dark *J-V* characteristics of the hole-only and electron-only devices are shown in Fig. 8(a) and 8(b) (see the device structures (17)-(20) in Fig. 1). For the hole-only devices, MoO_3 with high work function (WF) was inserted between α-6T and Al to facilitate hole injection from top Al because there is no hole injection barrier between MoO_3 (WF=5.68 eV [12]) and α-6T (IP=4.96-5.25). For the electron-only devices, Al was used as an electron-injecting electrode because there is no electron injection barrier between Al (WF≈4.0 eV [36]) and PTCBI (EA=4.32-4.47 eV) as well. The *J*-V curves were almost parallel shifted to a higher *J* in the whole *V* region by the uniaxial and multiaxial rubbing. The increases in *J* ≈17 times in the hole-only devices and ≈100 times in the electron-only devices were obtained, suggesting that hole mobility of α-6T and electron mobility of PTCBI are increased by the horizontal orientations. The reduction in R_S observed from the rubbed OSCs (Table 1) is additional proof of the increased hole and electron mobility. The increased hole and electron mobility enhances collection of holes and electrons by the electrodes and suppresses carrier recombination after exciton dissociation, resulting in the increase in FF and J_{SC} of the rubbed OSCs. It is noted that the increases in *L* (sec. 2.3) and *J* obtained from the rubbed PTCBI samples are somewhat overestimated in comparison with actual values inside the working OSCs

30

because PTCBI was not deposited on the oriented α-6T surface but directly deposited on the rubbed PTCBI surface.

The absorptivity spectra are easily calculated from the absorption spectra of Fig. 2(c) with a Lambert-Beer law. The absorptivity (1-transmittivity) is directly proportional to the photon number absorbed in the organic films. The increasing rates of the absorptivity after the uniaxial and multiaxial rubbing are ≈1.52 at 360 nm (where α-6T absorption is mainly presented) and ≈1.44 at 670 nm (where PTCBI absorption only is presented). On the other hands, the increasing rates of the IPCE (Fig. 3(c)) after the uniaxial and multiaxial rubbing are ≈2.32 at 360 nm and ≈1.63 at 670 nm, which are higher than those of the absorptivity. The difference in the increasing rate between the absorptivity and the IPCE probably originates from the increases in the L and the carrier mobility as demonstrated before.

Organic films absorb photons to create molecular excitons. Molecular excitons that diffuse and reach a heterojunction interface between the p-type and n-type layers are converted into charge transfer excitons, i.e., electron-hole pairs across the heterojunction interface. The charge transfer excitons separated by a built-in potential

become free electrons and holes, which are collected by electrodes and contribute to a photocurrent. The double horizontal orientations of α-6T and PTCBI demonstrated in this study improve these light absorption, exciton diffusion, and carrier collection processes at the same time. Moreover the observed increase in HOMO-LUMO difference allows V_{OC} to be increased. Therefore we infer that the OSC performance was improved by the uniaxial and multiaxial rubbing techniques.

3. Conclusions

We investigated the influence of molecular orientation of α-6T and PTCBI on OSC performance. We realized double horizontal orientations of α-6T and PTCBI by depositing α-6T and then PTCBI on uniaxially and multiaxially rubbed α-6T buffer surfaces due to quasi-homoepitaxial and quasi-heteroepitaxial growth effects. We obtained significant increases in V_{OC}, J_{SC}, FF, η, and long-term operation stability in the OSCs containing the horizontally oriented α-6T and PTCBI molecules. Results of several analyses of the α-6T and PTCBI films revealed that the horizontal orientations resulted in increases in absorbance, exciton diffusion length, HOMO/LUMO energy difference, and hole and electron transport, leading to the improved OSC performance. These results strongly demonstrate that the horizontal orientations caused by the

32

uniaxial and multiaxial rubbing are useful to enhance future OSC performance.

Acknowledgements

References

[1] G. Horowitz, D. Fichou, X. Peng, Z. Xu, F. Garnier, A field-effect transistor based on conjugated alpha-sexithienyl, Solid State Communications 72 (1989) 381-384.

[2] Y.C. Cheng, R.J. Silbey, D.A. da Silva Filho, J.P. Calbert, J. Cornil, J.L. Brédas, Three-dimensional band structure and bandlike mobility in oligoacene single crystals: A theoretical investigation, Journal of Chemical Physics. 118 (2003) 3764-3774.

[3] H. Yanagi, S. Okamoto, Orientation-controlled organic electroluminescence of *p*-sexiphenyl films, Applied Physics Letters 71 (1997) 2563-2565.

[4] P. Sullivan, T.S. Jones, A.J. Ferguson, S. Heutz, Structural templating as a route to improved photovoltaic performance in copper phthalocyanine/fullerene (C60) heterojunctions, Applied Physics Letters 91 (2007) 233114-1-233114-3.

[5] J. Frischeisen, D. Yokoyama, A. Endo, C. Adachi, W. Brütting, Increased light outcoupling efficiency in dye-doped small molecule organic light-emitting diodes with horizontally oriented emitters, Organic Electronics 12 (2011) 809-817.

[6] C. Videlot, A. El Kassmi, D. Fichou, Photovoltaic properties of octithiophene-based Schottky and p/n junction cells: Influence of molecular orientation, Solar Energy Materials & Solar Cells 63 (2000) 69-82.

[7] K. Ihm, B. Kim, T.-H. Kang, K.-J. Kim, M.H. Joo, T.H. Kim, S.S. Yoon, S. Chung, Molecular orientation dependence of hole-injection barrier in pentacene thin film on the Au surface in organic thin film transistor, Applied Physics Letters 89 (2006) 033504-1-033504-3.

[8] W. Chen, H. Huang, S. Chen, Y.L. Huang, X.Y. Gao, A.T.S. Wee, Molecular Orientation-Dependent Ionization Potential of Organic Thin Films, Chemistry of Materials 20 (2008) 7017-7021.

[9] S. Duhm, G. Heimel, I. Salzmann, H. Glowatzki, R.L. Johnson, A. Vollmer, J.P. Rabe, N. Koch, Orientation-dependent ionization energies and interface dipoles in ordered molecular assemblies, Nature Materials 7 (2008) 326-332.

[10] Y. Wang, T. Matsushima, H. Murata, A. Fleurence, Y. Yamada-Takamura, R. Friedlein, Molecular order, charge injection efficiency and the role of intramolecular polar bonds at organic/organic heterointerfaces, Organic Electronics 13 (2012) 1853-1858.

[11] C.J. Brabec, A. Cravino, D. Meissner, N.S. Sariciftci, T. Fromherz, M.T. Rispens, L. Sanchez, J.C. Hummelen, Origin of the Open Circuit Voltage of Plastic Solar Cells, Advanced Functional Materials 11 (2001) 374-380.

[12] T. Matsushima, H. Murata, Enhancement of hole injection and electroluminescence characteristics by a rubbing-induced lying orientation of alpha-sexithiophene, Journal of Applied Physics 112 (2012) 024503-1-024503-9.

[13] C.H. Cheng, J. Wang, G.T. Du, S.H. Shi, Z.J. Du, Z.Q. Fan, J.M. Bian, M.S. Wang, Organic solar cells with remarkable enhanced efficiency by using a CuI buffer to control the molecular orientation and modify the anode, Applied Physics Letters 97 (2010) 083305-1-083305-3.

[14] S. Ikeda, K. Saiki, Y. Wada, K. Inaba, Y. Ito, H. Kikuchi, K. Terashima, T. Shimada, Graphoepitaxy of sexithiophene and orientation control by surface treatment, Journal of Applied Physics 103 (2008) 084313-1-084313-9.

[15] J.C. Wittmann, P. Smith, Highly oriented thin films of poly(tetrafluoroethylene) as a substrate for oriented growth of materials, Nature (London) 352 (1991) 414-417.

[16] M. Era, T. Tsutsui, S. Saito, Polarized electroluminescence from oriented p-sexiphenyl vacuum-deposited film, Applied Physics Letters 67 (1995) 2436-2438.

[17] H. Tanaka, T. Yasuda, K. Fujita, T. Tsutsui, Transparent Image Sensors Using an Organic Multilayer Photodiode, Advanced Materials 18 (2006) 2230-2233.

[18] D. Yokoyama, A. Sakaguchi, M. Suzuki, C. Adachi, Horizontal molecular orientation in vacuum-deposited organic amorphous films of hole and electron

transport materials, Applied Physics Letters 93 (2008) 173302-1-173302-3.

[19] D. Yokoyama, Z.Q. Wang, Y.-J. Pu, K. Kobayashi, J. Kido, Z. Hong, High-efficiency simple planar heterojunction organic thin-film photovoltaics with horizontally oriented amorphous donors, Solar Energy Materials & Solar Cells 98 (2012) 472-475.

[20] R.R. Lunt, N.C. Giebink, A.A. Belak, J.B. Benziger, S.R. Forrest, Exciton diffusion lengths of organic semiconductor thin films measured by spectrally resolved photoluminescence quenching, Journal of Applied Physics 105 (2009) 053711-1-053711-7.

[21] S.-B. Rim, R.F. Fink, J.C. Schöneboom, P. Erk, P. Peumans, Effect of molecular packing on the exciton diffusion length in organic solar cells, Applied Physics Letters 91 (2007) 173504-1-173504-3.

[22] T. Matsushima, K. Shiomura, S. Naka, H. Murata, Optical, morphological, structural, electrical, molecular orientation, and electroluminescence characteristics of organic semiconductor films prepared at various deposition rates, Thin Solid Films 520 (2012) 2283-2288.

[23] P. Peumans, V. Bulović, S. R. Forrest, Efficient photon harvesting at high optical intensities in ultrathin organic double-heterostructure photovoltaic diodes, Applied

Physics Letters 98 (2011) 243307-1-243307-3.

[24] T. Matsushima, H. Murata, Enhanced charge-carrier injection caused by molecular orientation, Applied Physics Letters 98 (2011) 253307-1-253307-3.

[25] D. Oelkrug, H.-J. Egelhaaf, J. Haiber, Electronic spectra of self-organized oligothiophene films with "standing" and "lying" molecular units, Thin Solid Films 284-285 (1996) 267-270.

[26] H.-J. Egelhaaf, P. Bäiuerle, K. Rauer, V. Hoffmann, D. Oelkrug, Orientation and mobility in ultrathin oligothiophene films: UV-Vis, IR and fluorescence studies, Synthetic Metals 61 (1993) 143-146.

[27] Th. Főrster, Transfer mechanisms of electronic excitation, Discussions of the Faraday Society 27 (1959) 7-17.

[28] ϕ was roughly estimated to be $\approx$0.025% (α-6T) and $\approx$0.003% (PTCBI) from comparing absorbance at an excitation light wavelength and areas of PL spectra of α-6T and PTCBI with those of tris(8-hydroxyquinoline)aluminum (Alq$_3$) having η of 18% [Ref. 22]. ϕ of α-6T and PTCBI seemed not to be largely dependent on their molecular orientations.

[29] A. Shoustikov, Y. You, P.E. Burrows, M.E. Thompson, S.R. Forrest, Orange and red organic light-emitting devices using aluminum tris(5-hydroxyquinoxaline),

Synthetic Metals 91 (1997) 217-221.

[30] Z.Z. You, G.J. Hu, Refractive index, optical bandgap and oscillator parameters of organic films deposited by vacuum evaporation technique, Vacuum 83 (2009) 984-988.

[31] ε_A was calculated from absorption spectra and film thickness of PTCBI and CuPc acceptors deposited on fused silica substrates and their film density ρ and molecular mass. We used ρ=1.64 g cm^{-3} for CuPc, which was reported in following reference (H.-F. Xiang, Z.-X. Xu, V.A.L. Roy, C.-M. Che, P.T. Laia, Method for measurement of the density of thin films of small organic molecules, Review of Scientific Instruments 78 (2007) 034104-1-034104-5). To calculate ρ of PTCBI, PTCBI film of 100 nm (setting thickness) was vacuum-deposited on fused silica substrate with quartz crystal microbalance where ρ of 1.1 g cm^{-3}, tooling factor of 100%, and z-ratio of 1 were set. Since fused silica substrate was placed very close to quartz crystal microbalance inside vacuum evaporator, thickness of PTCBI deposited on quartz crystal microbalance is same as that of PTCBI deposited on fused silica surface. Actual thickness measured from PTCBI deposited on fused silica substrate was 84 nm from AFM analysis. Thus actual ρ of PTCBI was calculated to be 1.31 g cm^{-3} from product of setting ρ 1.1 g cm^{-3} and ratio of setting thickness 100

nm/actual thickness 84 nm.

[32] M. Granström, K. Petritsch, A.C. Arias, A. Lux, M.R. Andersson, R.H. Friend, Laminated fabrication of polymeric photovoltaic diodes, Nature (London) 395 (1998) 257-260.

[33] W. Wiedemann, L. Sims, A. Abdellah, A. Exner, R. Meier, K.P. Musselman, J.L. MacManus-Driscoll, P. Müller-Buschbaum, G. Scarpa, P. Lugli, L. Schmidt-Mende, Nanostructured interfaces in polymer solar cells, Applied Physics Letters 96 (2010) 263109-1-263109-3.

[34] K. Kanai, M. Honda, H Ishii, Y. Ouchi, K. Seki, Interface electronic structure between organic semiconductor film and electrode metal probed by photoelectron yield spectroscopy, Organic Electronics 13 (2012) 309-319.

[35] M.C. Scharber, D. Mühlbacher, M. Koppe, P. Denk, C. Waldauf, A.J. Heeger, C.J. Brabec, Design Rules for Donors in Bulk-Heterojunction Solar Cells -Towards 10% Energy-Conversion Efficiency, Advanced Materials 18 (2006) 789-794.

[36] H. Ishii, K. Sugiyama, E. Ito, K. Seki, Energy Level Alignment and Interfacial Electronic Structures at Organic/Metal and Organic/Organic Interfaces, Advanced Materials 11 (1999) 605-625.

Table 1. V_{OC}, J_{SC}, FF, η, R_S, and R_{SH} estimated from Fig. 3(a).

Sample	V_{OC} [V]	J_{SC} [mA cm^{-2}]	FF	η [%]	R_S [Ω cm^2]	R_{SH} [Ω cm^2]
Unrubbed OSC	0.38±0.01	1.70±0.09	0.61±0.01	0.40±0.02	41.2±4.7	(2.09±0.54)×10^3
Uniaxially rubbed OSC	0.68±0.01	2.80±0.07	0.65±0.02	1.23±0.05	29.2±2.9	(2.17±0.75)×10^3
Multiaxially rubbed OSC	0.68±0.01	2.73±0.15	0.64±0.02	1.18±0.06	26.4±4.7	(1.86±1.07)×10^3
Multiaxially rubbed OSC exposed to air	0.64±0.01	1.70±0.10	0.64±0.01	0.70±0.05	45.9±3.2	(1.63±0.82)×10^3

Figure captions

Fig. 1. Chemical structures of α-6T and PTCBI, sample preparation scheme and sample

structures used in this study. (2) and (3) represent top views of substrates where

arrows with numerals indicate rubbing directions and rubbing orders. For samples

(11)-(14), d of α-6T was varied from 20 to 50 nm and d of PTCBI was varied from

10 to 25 nm.

Fig. 2. UV-vis absorption spectra (unpolarization) of (a) α-6T sample (5) and (6) (Fig.

1) and (c) PTCBI samples (7) and (8) and substrate angle dependence of absorbance

of (b) α-6T samples at 360 nm and (d) PTCBI samples at 670 nm, which were

measured under normal incidence of unpolarized and polarized light to substrates,

respectively.

Fig. 3. (a) J-V characteristics under AM1.5 solar illumination of 100 mW cm^{-2}, (b)

substrate angle dependence of J_{SC}, and wavelength dependence of (c) IPCE and (d)

J_{SC}, which were measured from OSCs (9) and (10) of Fig. 1.

Fig. 4. Time stability of (a) V_{OC}, (b) J_{SC}, (c) FF, and (d) η of OSCs (9) and (10) (Fig. 1)

at initial optimum operation point under continuous solar light irradiation.

Fig. 5. Plots of PL_1/PL_2 ratios of (a) α-6T samples (11) and (12) (Fig. 1) and (b) PTCBI

samples (13) and (14) as function of thickness d. Symbols are experimental data and

solid curves are theoretical fitting used to estimate L.

Fig. 6. AFM images and corresponding cross section profiles of 50 nm α-6T films

deposited on (a) bare ITO substrate and ITO substrates covered with (b) uniaxially

and (c) multiaxially rubbed α-6T films.

Fig. 7. (a) Photoelectron yield spectra of samples (15) and (16) (Fig. 1) and (b)

energy-level diagrams of α-6T and PTCBI, which were measured from

photoelectron onset energy and absorption onset energy. Each straight line in (a) was

obtained with least-squares method.

Fig. 8. Dark J-V characteristics of (a) hole-only α-6T devices (17) and (18) (Fig. 1) and

(b) electron-only PTCBI devices (19) and (20).
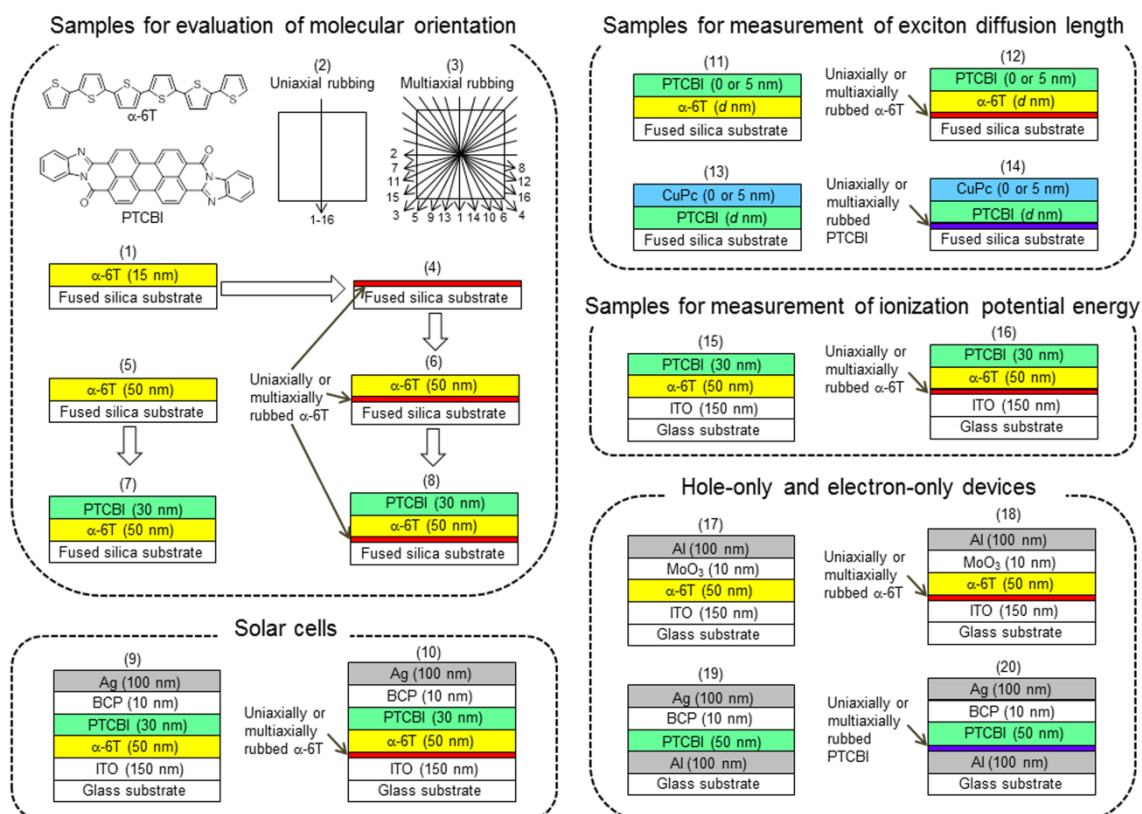
Fig. 1 (two-column figure)
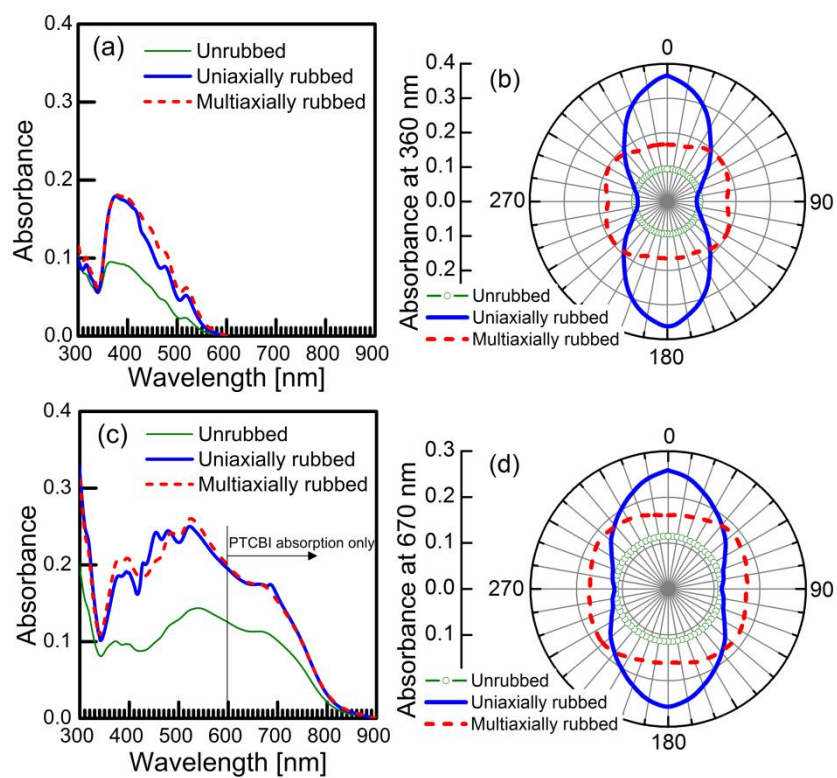
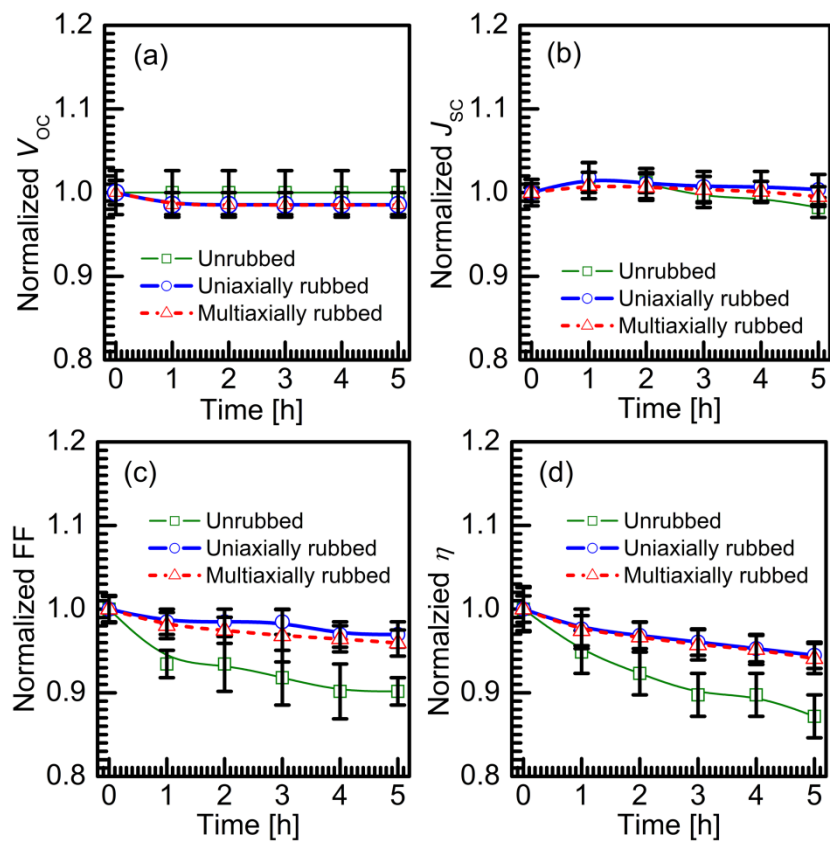Fig. 2 (two-column figure)
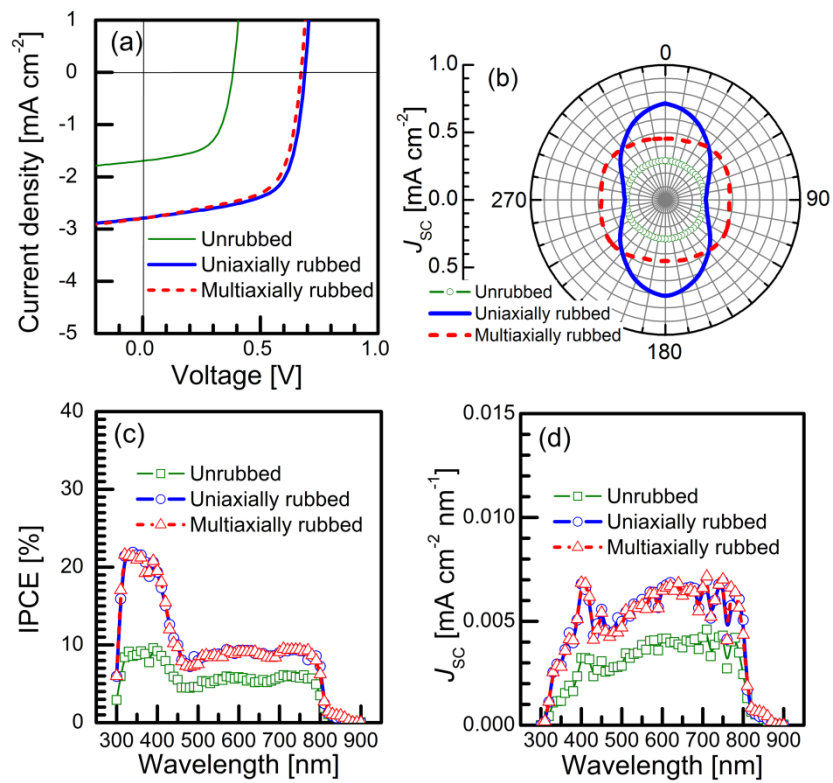
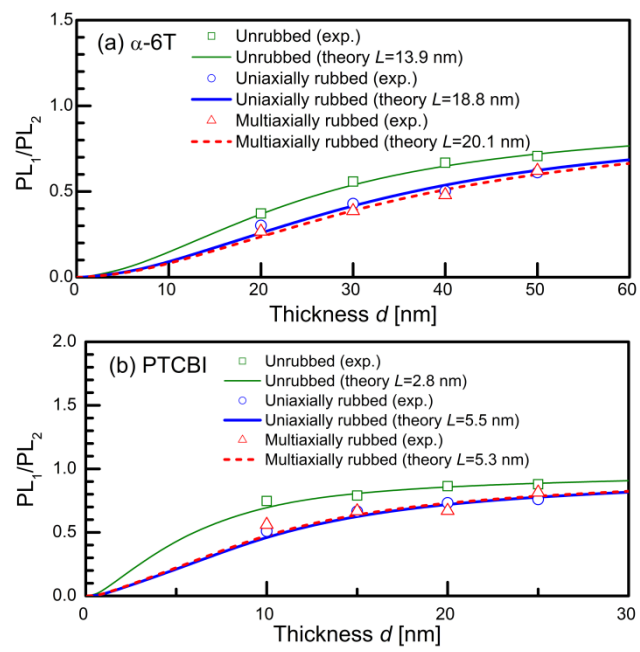Fig. 3 (two-column figure).

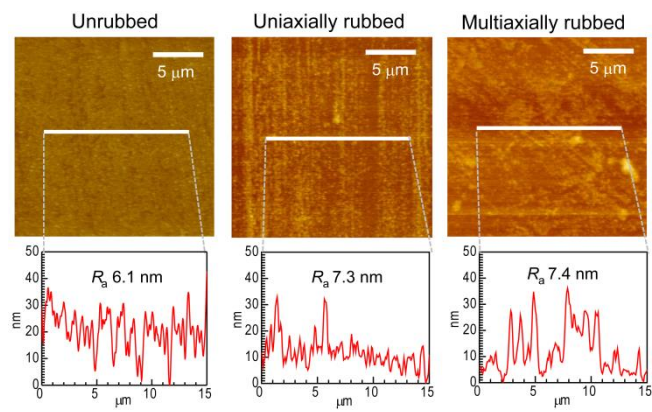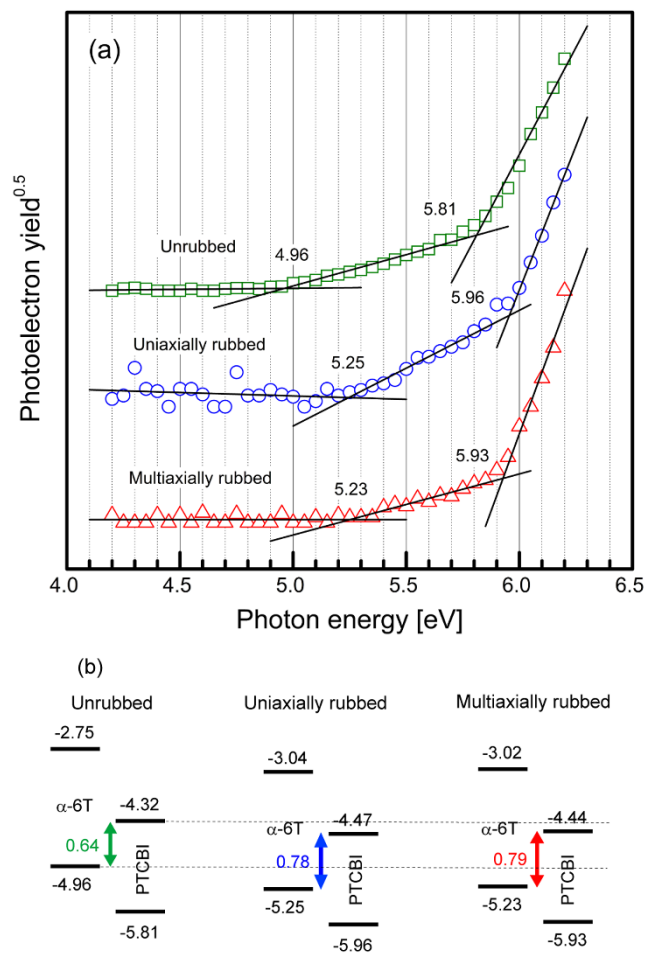Fig. 4 (two-column figure).
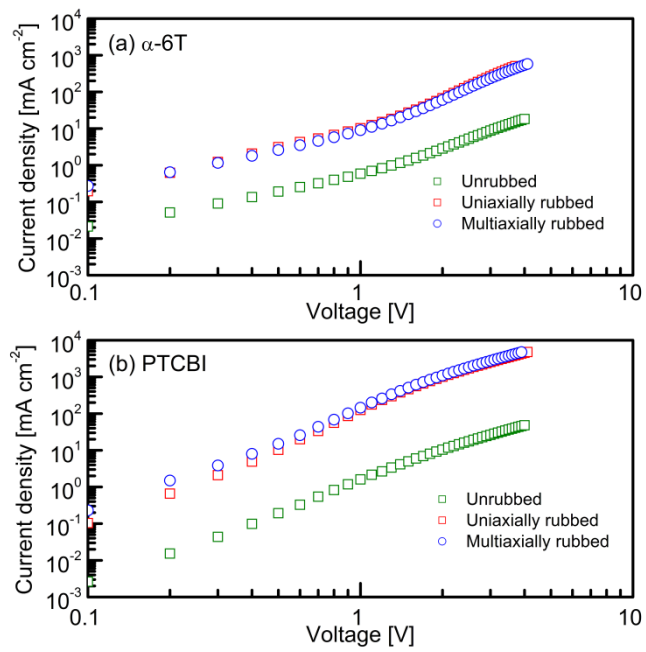
Fig. 5 (one-column figure).

Fig. 6 (one-column figure).

Fig. 7 (one-column figure).

Fig. 8 (one-column figure).